

Numerical Study of the Chiral Separation Effect in Two-Color QCD at Finite Density

P. V. Buividovich*

Department of Mathematical Sciences, University of Liverpool, Liverpool, L69 7ZL, UK

D. Smith†

*Institut für Theoretische Physik, Justus-Liebig-Universität, 35392 Giessen, Germany
Helmholtz Research Academy Hesse for FAIR (HFHF), Campus Giessen, 35392 Giessen, Germany and
Facility for Antiproton and Ion Research in Europe GmbH (FAIR GmbH), 64291 Darmstadt, Germany*

L. von Smekal‡

*Institut für Theoretische Physik, Justus-Liebig-Universität, 35392 Giessen, Germany and
Helmholtz Research Academy Hesse for FAIR (HFHF), Campus Giessen, 35392 Giessen, Germany*

(Dated: December 10th, 2020)

We study the Chiral Separation Effect (CSE) in finite-density $SU(2)$ lattice gauge theory with dynamical fermions. We find that the strength of the CSE is close to that for free quarks in most regions of the phase diagram, including the high-temperature quark-gluon plasma phase, the low-temperature phase with spontaneously broken chiral symmetry, and the diquark condensation phase which is specific for the $SU(2)$ gauge theory. The CSE is significantly suppressed only at low temperatures and low densities, where the chemical potential is roughly less than half of the pion mass. This suppression can be approximately described by assuming that the CSE current is proportional to the charge density, rather than to the chemical potential, as suggested in the literature [Phys. Rev. D **97**, 085020 (2018)]. We also provide an upper bound on the contribution of disconnected fermionic diagrams to the CSE, which is consistent with zero within our statistical errors and small compared to that of the connected diagrams.

I. INTRODUCTION

Anomalous transport phenomena are transport responses of quantum matter which originate in quantum anomalies, inevitable violations of classical symmetries upon quantization [1, 2]. In particular, in strongly interacting matter described by Quantum Chromodynamics (QCD) the classical symmetry between left-handed and right-handed fermions is violated by the Adler-Bell-Jackiw axial anomaly [3]. This violation manifests itself in the infamous Chiral Magnetic Effect [4] - the generation of an electric current along a magnetic field in chirally imbalanced matter - as well as the closely related Chiral Separation Effect (CSE) [5, 6] - the generation of an axial current along a magnetic field in a dense medium (see Fig. 1).

In the last decade, anomalous transport phenomena in QCD matter were systematically and intensely studied in heavy-ion collision experiments at the RHIC [7] and LHC [8] colliders, and will also be studied at the NICA collider [9]. These studies are not conclusive yet due to large background effects, which contaminate the signatures of anomalous transport [8, 10–14]. A dedicated run with isobar nuclei has been recently completed at RHIC in order to disentangle these background effects [7, 15], and the produced experimental data is currently being analyzed [16].

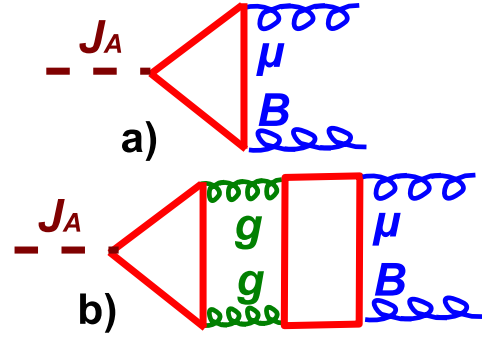


FIG. 1. a) Feynman diagrams which contribute to the Chiral Separation Effect at leading order and b) one of the possible corrections to it in a gauge theory with dynamical fermions.

Just as the viscosity of the quark-gluon plasma is related to hadronic elliptic flow [17], anomalous transport coefficients characterizing the strengths of the Chiral Magnetic and Chiral Separation Effects can be related to correlations of angular distributions of oppositely charged hadrons in heavy-ion collisions [18, 19].

One of the most popular ways to interpret experimental data on these correlations relies on the anomalous-viscous fluid dynamics (AVFD) framework [20–22]. AVFD is based on anomalous hydrodynamics [23–25] which incorporates anomalous transport along with more conventional transport responses such as viscosity and electric conductivity. Hydrodynamic simulation codes which include anomalous transport phenomena on an event-by-event basis are currently being ac-

* pavel.buividovich@liverpool.ac.uk

† d.smith@gsi.de

‡ lorenz.smekal@physik.uni-giessen.de

tively developed [21, 26–28] and are becoming more and more realistic.

The anomalous hydrodynamic description of QCD matter requires the values of anomalous transport coefficients as an input. For a single-component chiral fluid, anomalous transport coefficients are fixed by thermodynamic consistency [24, 29]. On the other hand, in a quark-gluon plasma (nearly) chiral quarks interact with dynamical non-Abelian gauge fields, which themselves behave as a viscous fluid and in fact dominate the hydrodynamic flow. When interactions with dynamical gauge fields are present, all anomalous transport coefficients might receive both perturbative [30] (see Fig. 1) as well as non-perturbative [6, 31–35] corrections. However, at present not much is known about the magnitude of these corrections.

In a few lattice gauge theory simulations, the Chiral Magnetic [36] and Chiral Vortical [37] Effects were studied by measuring the responses of naively discretized axial currents and energy momentum tensors to constant external magnetic or axial magnetic fields (the study [37] of the Chiral Vortical Effect used a trick to replace rotation by a background axial gauge field). In both works [36, 37] the CME and CVE transport coefficients were found to be 5 to 20 times smaller than those obtained for free fermions, both in high- and in low-temperature phases. If the corrections in the full gauge theory should indeed have the effect to make the anomalous transport responses so small, they might well be unobservable in current heavy-ion collision experiments.

However, the works [36, 37] used non-chiral lattice fermions with non-conserved currents and an energy-momentum tensor without proper renormalization. On the other hand, a numerical study of the Chiral Separation Effect in quenched $SU(3)$ lattice gauge theory with exactly chiral overlap fermions and properly defined axial current [38] found no noticeable corrections to the free fermion result,

$$j_i^A = \frac{\mu C_{em} N_c}{2\pi^2} B_i \equiv \sigma_{\text{CSE}}^0 B_i, \quad (1)$$

where $j_i^A = \sum_f \bar{q}_f \gamma_5 \gamma_i q_f$ is the axial current density with quark fields \bar{q}_f, q_f of flavor f and N_c colors, μ is the fermion chemical potential, B_i is the magnetic field, and $C_{em} = \sum_f Q_f$ is the electromagnetic charge factor in which Q_f denotes the electric charge of quark flavor f . The result (1) corresponds to the triangular diagram in Fig. 1 a). To simplify notation, in what follows we assume that C_{em} , which appears in all formulae as a simple prefactor, is equal to unity: $C_{em} = 1$. The correct value of C_{em} can be restored in all results in an obvious way.

In this work we study the Chiral Separation Effect in the full gauge theory with dynamical fermions, taking into account the contributions of virtual fermion loops and disconnected fermionic diagrams like the one in Fig. 1 b). These contributions are expected to modify the free fermion result (1) and are thus important to know for the detectability of the Chiral Separation Effect in heavy-ion collisions. Rather than studying the

theoretically clean, but rather academic, limit of exactly chiral quarks, we address the fate of the CSE in a more realistic setup with finite quark and pion masses and at finite temperatures in the vicinity of the chiral crossover. While giving some general insight into the magnitude of non-perturbative corrections to anomalous transport coefficients, this might also help to estimate the observable consequences of the CSE, such as the electric quadrupole moment of the quark-gluon plasma [39] due to Chiral Magnetic Waves [40].

Since the CSE is a feature of finite-density fermions, studying it in QCD would require simulations at finite baryon density, which are complicated by the infamous fermion-sign problem [41]. With current simulation methods one could only obtain first-principle lattice QCD results for $\mu/T \ll 1$. In particular, a study of the CSE in chiral effective field theory [35] suggests that for sufficiently low temperatures it is suppressed at $\mu < m_\pi/2$, where m_π is the pion mass. However, this is precisely the region where the QCD sign problem is expected to be small, and there are little chances to obtain any reliable results outside of this region in near future.

In this work we circumvent the fermion sign problem by using two-color QCD, i.e. the $SU(2)$ gauge theory with $N_f = 2$ light quark flavours instead of QCD. The path integral weight is manifestly positive in this case, thus the sign problem is absent and the theory can be simulated at finite density. The $SU(2)$ gauge theory is expected to be qualitatively similar to QCD at small densities $\mu < m_\pi/2$ [42, 43]. In this regime there is a conventional QCD-like chiral crossover at some finite temperature, which separates the quark-gluon plasma phase and the hadron gas phase dominated by light pion states [44–49]. We expect that due to this qualitative similarity our numerical study of the CSE in $SU(2)$ gauge theory is also at least qualitatively relevant for real QCD at small densities.

At larger densities, for $\mu > m_\pi/2$, $SU(2)$ gauge theory is no longer similar to QCD, since the chiral condensate $\langle \bar{q}q \rangle$ is rotated into the diquark condensate $\langle qq \rangle$. Diquarks are bound states of two quarks which are color singlets and hence “bosonic baryons” in the $SU(2)$ gauge theory. Instead of the first-order liquid-gas transition of nuclear matter, one therefore observes Bose-Einstein condensation together with a BEC-BCS crossover inside the diquark condensation phase [50, 51]. Similarity to QCD, although at a different conceptual level, can be again expected at very large densities and low temperatures, in the conjectured quarkyonic and color-superconducting phases [52, 53].

II. LINEAR RESPONSE APPROXIMATION FOR THE CHIRAL SEPARATION EFFECT

Within linear response theory, the Chiral Separation Effect is characterized by the correlator of vector and axial-vector currents $\langle j_1^A(k_3) j_2^V(-k_3) \rangle$, where the only nonzero momentum component is the spatial component

k_3 [54]. At small momenta this correlator behaves as

$$\langle j_1^A(k_3) j_2^V(-k_3) \rangle = \sigma_{\text{CSE}} k_3, \quad (2)$$

where σ_{CSE} is the anomalous transport coefficient in (1) characterizing the strength of the CSE. For free fermions,

$$\sigma_{\text{CSE}} = \sigma_{\text{CSE}}^0 = \frac{\mu N_c}{2\pi^2}. \quad (3)$$

It is therefore convenient to define a momentum-dependent transport coefficient $\sigma_{\text{CSE}}(k)$ as

$$\sigma_{\text{CSE}}(k_3) \equiv \langle j_1^A(k_3) j_2^V(-k_3) \rangle / k_3. \quad (4)$$

In the low-momentum hydrodynamic regime, the anomalous transport coefficient σ_{CSE} in (1) is given by the zero-momentum limit of $\sigma_{\text{CSE}}(k)$.

For exactly chiral fermions which may interact, but not with other dynamical degrees of freedom (like dynamical gauge fields), σ_{CSE} is expected to be universal and equal to the free fermion result due to the relation with the Adler-Bell-Jackiw axial anomaly [5]. However, corrections are still possible for nonzero quark mass [6] and due to fermionic disconnected diagrams like 1b) on Fig. 1. As calculations of [6] suggest, corrections to the CSE can be related to the amplitude $g_{\pi^0\gamma\gamma}$ for the $\pi_0 \rightarrow \gamma\gamma$ decay:

$$\sigma_{\text{CSE}} = \frac{\mu N_c C_{em}}{2\pi^2} (1 - g_{\pi^0\gamma\gamma} + O(\mu)). \quad (5)$$

Within the linear sigma model $g_{\pi^0\gamma\gamma} = \frac{7\zeta(3)m^2}{4\pi^2 T^2}$, where m is the constituent quark mass.

Another calculation of the flavor non-singlet CSE axial current j_A^a generated by a finite isospin chemical potential was carried out within chiral effective field theory in [35]. It suggests that in the low-temperature phase, where the CSE current is saturated by pions, σ_{CSE} is proportional to the isospin charge density ρ_V^a rather than the isospin chemical potential,

$$\vec{j}_A^a = \frac{N_c \text{Tr}(Q)}{4\pi^2 f_\pi^2} \rho_V^a \vec{B}. \quad (6)$$

While this calculation is not directly applicable to the flavor-singlet axial current in (1) and (5), at least in the large- N_c limit the flavor-singlet axial current should behave similarly to the flavor non-singlet one [55]. Our numerical results presented in Section IV below suggest that a parametrization similar to (6) might also work at finite density in the $SU(2)$ gauge theory with dynamical fermions.

III. LATTICE SETUP

In this work we use the same lattice setup and the same ensembles of gauge field configurations as in our recent work [44], so here we will provide only a brief summary. We use the standard Hybrid Monte-Carlo algorithm with a tree-level improved Symanzik gauge action and $N_f =$

2 flavours of mass-degenerate rooted staggered fermions with bare lattice quark mass $am_q^{\text{stag}} = 5 \cdot 10^{-3}$. This yields a pion mass of $am_\pi^{\text{stag}} = 0.158 \pm 0.002$ and the ratio of pion to ρ -meson mass $m_\pi/m_\rho = 0.40 \pm 0.05$.

Our lattices have spatial sizes $L_s = 24$ ($am_\pi L_s = 3.8$) and $L_s = 30$ ($am_\pi L_s = 4.7$) and varying temporal extent $L_t = 4, 6, \dots, 22$ to control temperature $T = 1/aL_t$. We use a single value of the lattice gauge coupling $\beta = 1.7$, thus working in a fixed-scale approach, which significantly simplifies the analysis of renormalization of lattice observables.

Most of our low-temperature ensembles with $L_t \geq 12$ were generated with a small diquark source λqq in the action with $a\lambda = 5 \cdot 10^{-4}$ in order to facilitate diquark condensation, which would otherwise be impossible in a finite volume. This diquark source has very little effect on current-current correlators outside of the diquark condensation phase [44], see also Fig. 4. Estimates of phase boundaries based on our data sets are shown in Fig. 2 (see [44] for full details).

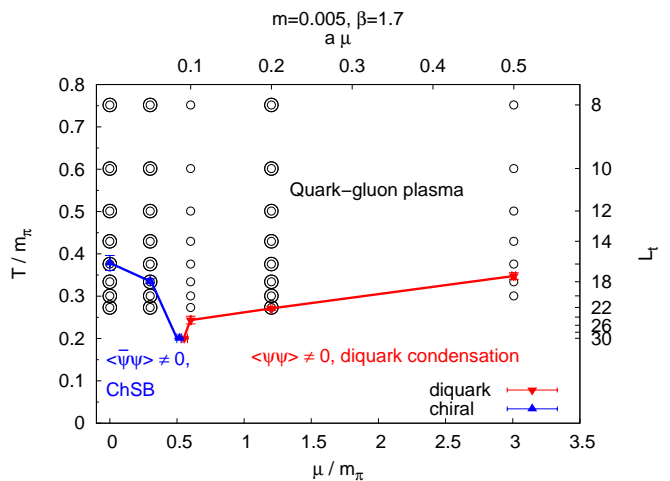


FIG. 2. Numerical estimate of the phase diagram of finite-density $SU(2)$ gauge theory with $N_f = 2$ rooted staggered fermions. Blue and red points correspond to inflection points in the L_t dependence of the chiral and diquark condensates, respectively. Configuration sets with lattice size $L_s = 24$ only are shown as empty circles, and sets with both $L_s = 24$ and $L_s = 30$ are shown as double circles.

We use Domain Wall (DW) and Wilson-Dirac (WD) valence fermions to measure the correlators of axial and vector currents in (2). On the one hand, for DW fermions the renormalization factor Z_A for the flavour-singlet axial current is expected to deviate from unity by at most few percent [56], which is below our the statistical uncertainty of our Monte-Carlo simulations (and also well below experimental uncertainties). On the other hand, DW fermions are computationally very expensive, and we use the cheaper WD fermions to produce results with better precision covering more points on the phase diagram. A comparison between the results obtained with DW and WD fermions further demonstrates the smallness of axial

current renormalization. We do not use staggered valence fermions in order to avoid artifacts related to unphysical taste symmetry. Such a mixed lattice action with staggered sea fermions and DW valence fermions has already been used in a number of studies of the nucleon axial charge [56, 57].

We tune the bare quark masses $am_q^{DW} = 0.01$ and $am_q^{WD} = -0.21$ in the DW/WD Dirac operators to match the pion mass $am_\pi^{stag} = 0.158 \pm 0.002$ obtained with staggered valence quarks. To improve the chiral properties of DW and WD fermions without using much finer and larger lattices, we follow [57] and use HYP smearing [58] for gauge links in the DW and WD Dirac operators. For DW fermions the lattice size in the fifth dimension is $L_5 = 16$, which is typically sufficient to suppress additive mass renormalization [56, 57].

For WD fermions, we use the conserved vector current

$$\begin{aligned} j_{z,\mu}^V &= \sum_{x,y} \bar{q}_x (j_{z,\mu})_{x,y} q_y, \\ (j_{z,\mu})_{x,y} &\equiv \frac{\partial D_{xy}}{\partial \theta_{z,\mu}} \\ &= iP_\mu^+ U_{z,\mu} \delta_{x,z} \delta_{y,z+\hat{\mu}} - iP_\mu^- U_{z,\mu}^\dagger \delta_{x,z+\hat{\mu}} \delta_{y,z}, \end{aligned} \quad (7)$$

where D_{xy} is the Dirac operator, x, y, z, \dots label lattice sites, γ_μ are the Euclidean gamma-matrices, with $P_\mu^\pm = (1 \pm \gamma_\mu)/2$, $U_{z,\mu}$ are the $SU(2)$ -valued link variables, $\hat{\mu}$ denotes the unit lattice vector in the direction μ , and $\theta_{z,\mu}$ is an external $U(1)$ gauge field. We also use the conventional point-split definition of the axial current for WD fermions [59],

$$\begin{aligned} (j_{z,\mu}^A)_{x,y} &\equiv \frac{\partial D_{xy}}{\partial \theta_{z,\mu}} \\ &= i\gamma_\mu \gamma_5 U_{z,\mu} \delta_{x,z} \delta_{y,z+\hat{\mu}} - i\gamma_\mu \gamma_5 U_{z,\mu}^\dagger \delta_{x,z+\hat{\mu}} \delta_{y,z}. \end{aligned} \quad (8)$$

For DW fermions, the four-dimensional vector and axial currents are defined in the standard way by summing the five-dimensional conserved current over the fifth dimension. For the vector current a unit weight is used, for the axial current the summation weight changes from +1 to -1 in the middle of the lattice extending in fifth dimension [60]. The five-dimensional conserved current has a form similar to (7), except that μ takes five values and x, y, z live on the five-dimensional lattice with open boundary conditions along the fifth dimension.

We measure the contributions of both connected and disconnected fermionic diagrams to the axial-vector current-current correlator in (2). In coordinate space these contributions are:

$$\begin{aligned} \langle j_{x,\mu}^A j_{y,\nu}^V \rangle_{conn} &= \langle \text{Tr} (j_{x,\mu}^A D^{-1} j_{y,\nu}^V D^{-1}) \rangle, \\ \langle j_{x,\mu}^A j_{y,\nu}^V \rangle_{disc} &= \langle \text{Tr} (j_{x,\mu}^A D^{-1}) \text{Tr} (j_{y,\nu}^V D^{-1}) \rangle, \end{aligned} \quad (9)$$

where the traces are taken over the lattice site, spinor and color indices of the quark fields \bar{q}, q . The disconnected contribution is measured using standard stochastic estimation techniques. After measuring $\langle j_{x,\mu}^A j_{y,\nu}^V \rangle_{conn}$ and

$\langle j_{x,\mu}^A j_{y,\nu}^V \rangle_{disc}$ in coordinate space, we perform a discrete Fourier transform to obtain the momentum-space correlators which enter the linear response relations (2).

IV. NUMERICAL RESULTS

In Fig. 3 we present our lattice results for the momentum dependent CSE transport coefficient $\sigma_{\text{CSE}}(k)$ defined in (4). For comparison, we combine the results obtained with DW and WD fermions, and with the spatial lattice sizes $L_s = 24$ and $L_s = 30$. For WD fermions on the $L_s = 24$ lattices we show the contributions (9) and (10) of both connected and disconnected fermionic diagrams, for other data sets only the connected contributions are shown. We also compare the gauge theory results with the results obtained for free WD quarks on same lattices.

For the free WD quarks, we use a bare quark mass of $am_q^{WD} = 0.01$ (as compared to $am_q^{WD} = -0.21$ in the full gauge theory), since for free quarks there is obviously no mass renormalization. Therefore, in this case we choose the same bare quark mass as for the DW fermions, for which mass renormalization is expected to be weak.

In our calculations we also combine results obtained with zero diquark source λ at high temperatures ($L_t < 14$) and with $a\lambda = 5 \cdot 10^{-4}$ at low temperatures ($L_t \geq 14$). In Fig. 4 we demonstrate that for these two values of λ the CSE transport coefficients $\sigma_{\text{CSE}}(k)$ are practically indistinguishable.

We see from Fig. 3 that for most values of temperature and chemical potential the momentum-dependent CSE transport coefficient $\sigma_{\text{CSE}}(k)$ is very close to the corresponding free-fermion result for all momenta. An explicit calculation of $\sigma_{\text{CSE}}(k)$ for free quarks at finite temperature in the continuum is sketched in Appendix A. The results of this continuum calculation are shown in all plots of Fig. 3 as black solid lines. We note that $\sigma_{\text{CSE}}(k)$ only becomes noticeably smaller than the free quark result at low temperatures and small values of chemical potential, less than half the pion mass (see e.g. the plot for $L_t = 20$ and $a\mu = 0.05$ corresponding to $\mu = 0.32 m_\pi$ in Fig. 3). In this regime the $SU(2)$ gauge theory is expected to be qualitatively similar to real QCD, thus the observed suppression of the CSE in the confined and chirally broken phase is also likely to happen in low-temperature, low-density QCD.

The contributions from disconnected fermionic diagrams appear to be consistent with zero within statistical errors for all values of chemical potential and temperature. The upper bound which we are able to set on these disconnected contributions appears to be least strict for low temperatures and small μ - that is, exactly in the corner of the phase diagram where also the connected contributions deviate most strongly from the free quark result (see Fig. 3, plot for $L_t = 20$ and $a\mu = 0.05$). We note, however, that the calculation of axial-vector current-current correlators is most difficult precisely in

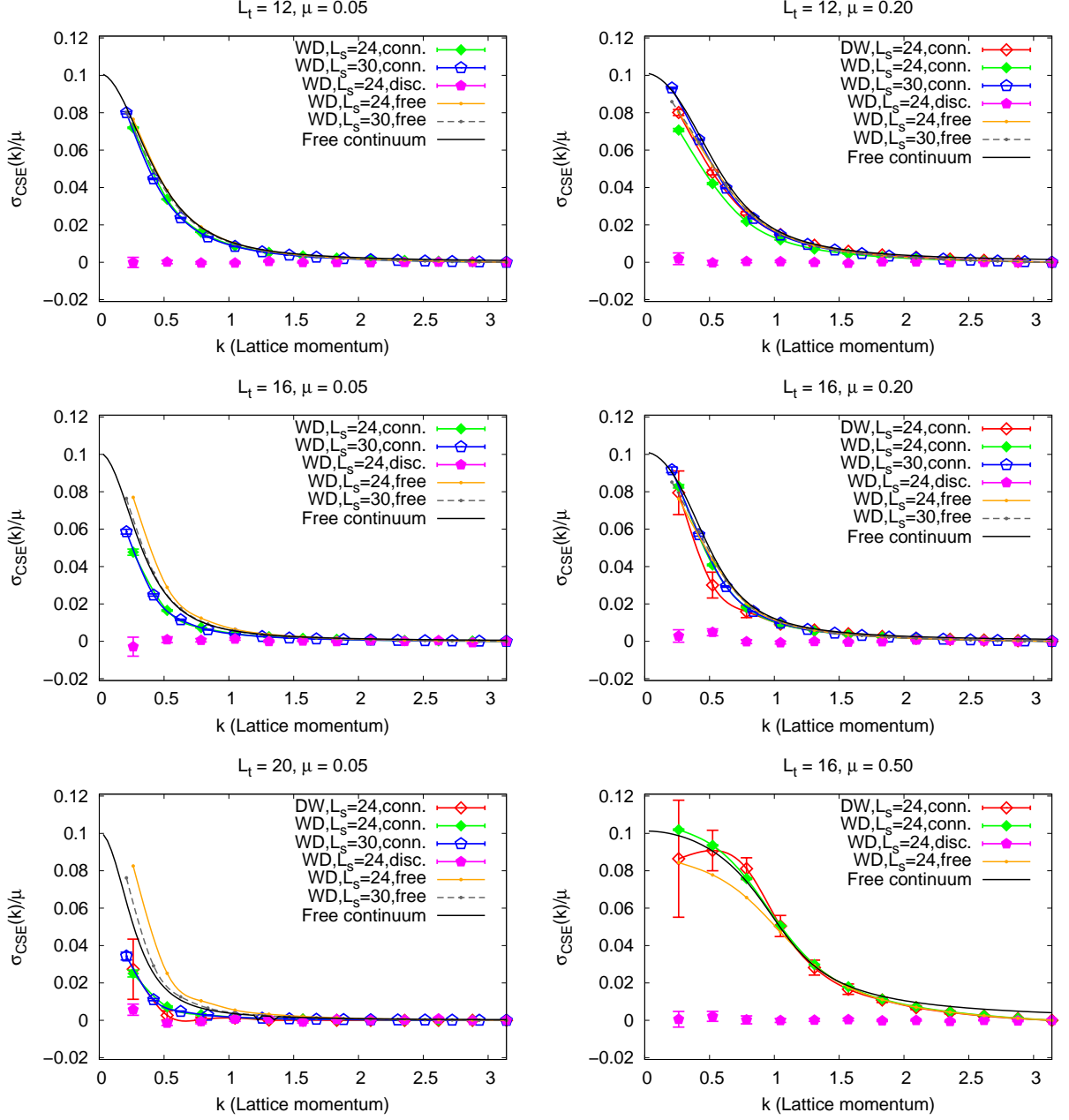


FIG. 3. Momentum-dependent CSE transport coefficient $\sigma_{\text{CSE}}(k)$ as function of lattice momentum k at selected temperatures and chemical potentials, corresponding roughly to: $\mu \simeq 0.32 m_\pi$ for three temperatures across the chiral transition (left column), as well as $\mu \simeq 1.3 m_\pi$ and $\mu \simeq 3.2 m_\pi$ for temperatures approaching the boundary of diquark condensation from above (right column).

this regime, since because of the small chemical potential the CSE signal is also small compared to the statistical fluctuations.

Moreover, we also note that the values of $\sigma_{\text{CSE}}(k)$ calculated with Wilson-Dirac (WD) and Domain Wall (DW) fermions appear to be very close to each other. This suggests that the effect of multiplicative renormalization of the axial-current operator is small and plays a minor role in comparison with our statistical errors, as well as with any systematic and statistical uncertainties in the

experimental detection of anomalous transport phenomena. Indeed, the renormalization factor for the axial singlet current typically appears to be close to unity on fine lattices with sufficiently light pions, especially for Domain Wall fermions [56, 57]. For these reasons, we have not determined the precise value of Z_A in this work.

In order to systematically investigate the CSE transport coefficient $\sigma_{\text{CSE}}(k)$ in the low-momentum limit, which is most relevant for anomalous hydrodynamics [54], in Fig. 5 we illustrate the temperature dependence of

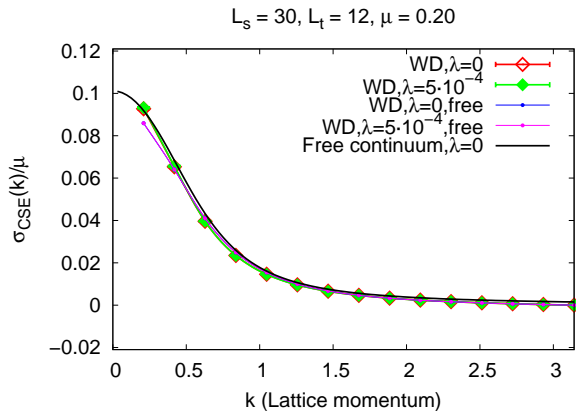


FIG. 4. CSE transport coefficient $\sigma_{\text{CSE}}(k)$ for different values of the diquark source λ .

$\sigma_{\text{CSE}}(k)$ at the smallest nonzero value of the lattice momentum, $ka = 2\pi/L_s$ at different values of the chemical potential μ , and compare it with the corresponding results for free quarks on lattices of the same size. In order to check whether the formula similar to (6) might describe our numerical results, we also show the appropriately rescaled charge density (in lattice units) along with $\sigma_{\text{CSE}}(k \rightarrow 0)$.

Again, we observe that $\sigma_{\text{CSE}}(k \rightarrow 0)$ becomes significantly smaller than the free quark result only at low temperatures and small values of μ , in the chirally broken and confined phase which should be dominated by the pions. The data for $L_s = 24$ and $L_s = 30$ appear to be reasonably close, thus suggesting that the suppression of the CSE in this phase is not a finite-volume artifact. Comparing the data for σ_{CSE} with the temperature dependence of the charge density, we furthermore observe that at low temperatures ($L_t \gtrsim 16$) and $a\mu \lesssim 0.20$ the dependence of $\sigma_{\text{CSE}}(k \rightarrow 0)$ on both μ and temperature can be approximately described by a formula of the form (6), except with a flavour-singlet current and chemical potential:

$$\begin{aligned} \sigma_{\text{CSE}}(k \rightarrow 0, \mu) &= \alpha \rho_V(\mu), \\ \vec{j}_A &= \alpha \rho_V(\mu) \vec{B}, \end{aligned} \quad (11)$$

where the constant α is about $\alpha \approx 10 a^2$ in lattice units, i.e. for our particular value of lattice spacing (this does not imply that α scales as a^2 with the lattice spacing a). With our value of the vacuum pion mass, we may write $\alpha \approx 1/(2m_\pi)^2$. According to (6), the coefficient α in (11) should be related to the pion decay constant f_π via $\alpha = N_c/(2\pi f_\pi)^2$. Using our estimate $\alpha a^{-2} \approx 10$, from this relation we roughly estimate $a f_\pi \approx 0.07$, which has a reasonable order of magnitude compared to the pion mass $am_\pi = 0.158$. Only for $a\mu = 0.50$ we observe a significant decrease of the coefficient α down to $\alpha \approx 2 a^2$ which would be in line with a pion mass that increases with μ as expected in the diquark condensation phase.

In order to present further evidence for the scaling of

σ_{CSE} with ρ_V , in Fig. 6 we show the dependence of the ratios $\sigma_{\text{CSE}}(k \rightarrow 0)/\mu$ (on the left) and $\sigma_{\text{CSE}}(k \rightarrow 0)/\rho_V$ (on the right) on the chemical potential μ at different temperatures. Data points appear to collapse better onto a single curve for the ratio $\sigma_{\text{CSE}}(k \rightarrow 0)/\rho_V$.

While these observations give some qualitative support to the formula (11), because of a conceptually different status of axial-singlet and axial-non-singlet currents in low-energy chiral effective theory, at the quantitative level one can expect further corrections to this formula. A general conclusion which we can make based on our results is that the CSE should be suppressed for values of the chemical potential roughly smaller than the pion mass. At higher temperatures and densities, the CSE transport coefficient should approach its value for free quarks.

V. CONCLUSIONS

To summarize, we have found that in a gauge theory with dynamical fermions the Chiral Separation Effect is close to the free fermion results in all regions of the phase diagram, including the high-temperature quark-gluon plasma phase, the low-temperature phase with spontaneously broken chiral symmetry and the diquark condensation phase. This conclusion agrees with the results of a previous study [38] in quenched $SU(3)$ lattice gauge theory with exactly chiral valence quarks (thus formally at zero pion mass). The CSE only appears to be suppressed in one corner of the phase diagram, namely at low temperatures and low densities, where chiral symmetry is spontaneously broken and the chemical potential is roughly below the half of the pion mass. Exactly this regime of $SU(2)$ gauge theory is similar to the low-temperature, low-density phase of real finite-density QCD, thus our findings should be also relevant for real QCD at least qualitatively.

The suppression of the CSE at low densities and temperatures can be approximately described if one assumes that the CSE current is proportional to the charge density rather than to the chemical potential, as in equation (6). While the formula (6) was derived in [35] for the axial non-singlet current, we see that at the qualitative level it also applies to the axial singlet current, which has a different status within the chiral effective theory.

Contributions of disconnected fermionic diagrams to the Chiral Separation Effect appear to be consistent with zero within our statistical errors. The latter are relatively large at low temperatures and densities. For this reason we cannot rule out that the disconnected contribution might become important when the connected one is strongly suppressed. This scenario would certainly be interesting from a theoretical viewpoint. However, as the sum of both contributions still appears to be small as compared to the free massless fermion result, it is probably not very relevant for the experimental detection of anomalous transport phenomena.

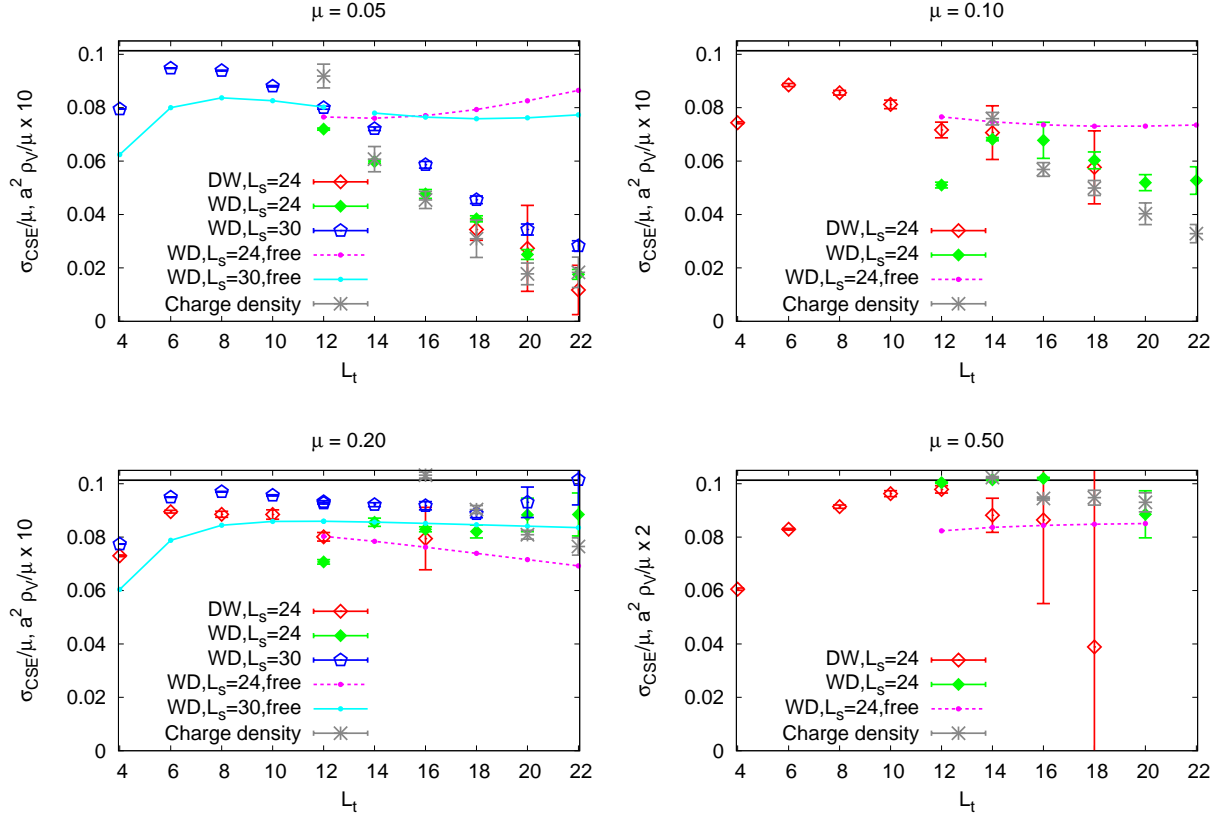


FIG. 5. Low-momentum limit of the CSE transport coefficient $\sigma_{\text{CSE}}(k \rightarrow 0)$ as a function of temporal lattice size (inverse temperature in lattice units) at different values of the chemical potential. The solid black lines correspond to $\sigma_{\text{CSE}}(k \rightarrow 0) = \sigma_{\text{CSE}}^0 = \mu N_c / 2\pi^2$ for free massless quarks in the continuum.

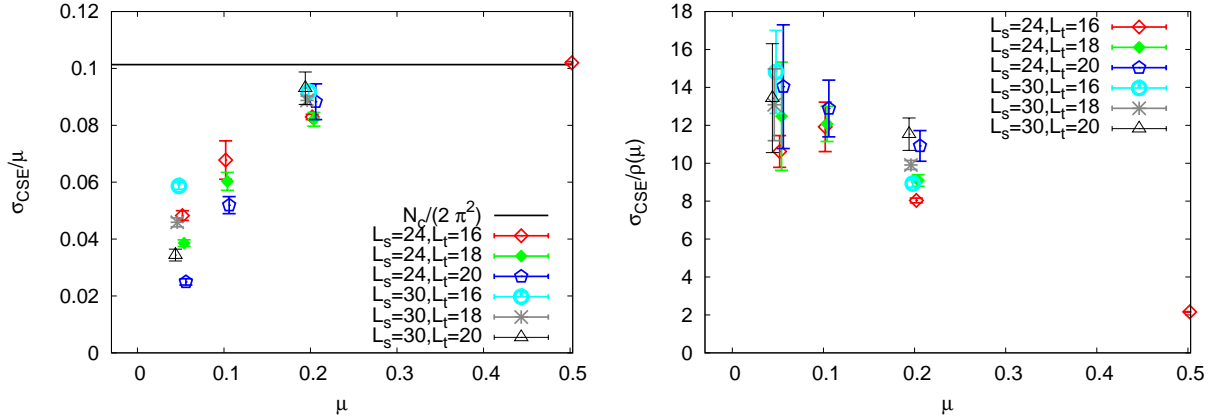


FIG. 6. Ratios of the low-momentum CSE transport coefficients σ_{CSE} with chemical potential μ (left) and charge density ρ_V (right).

One potential source of systematic errors in our study is the multiplicative renormalization of the axial current. However, comparison of the data obtained with Domain Wall and Wilson-Dirac fermions, as well as previous lattice studies of axial current renormalization, suggest that the renormalization effects are small.

ACKNOWLEDGMENTS

The work of P. B. was supported by the Heisenberg Fellowship from the German Research Foundation, project BU2626/3-1. D. S. received funding from the European Union's Horizon 2020 research and innovation pro-

gramme under grant agreement No. 871072, also known as CREMLINplus (Connecting Russian and European Measures for Large-scale Research Infrastructures).

This work was performed using the Cambridge Service for Data Driven Discovery (CSD3), part of which is operated by the University of Cambridge Research Computing on behalf of the STFC DiRAC HPC Facility (www.dirac.ac.uk). The DiRAC component of CSD3

was funded by BEIS capital funding via STFC capital grants ST/P002307/1 and ST/R002452/1 and STFC operations grant ST/R00689X/1. DiRAC is part of the National e-Infrastructure.

The simulations were also performed on the GPU cluster at the Institute for Theoretical Physics at Giessen University. Many thanks to Dominik Schweitzer for keeping this cluster alive during #JLUoffline.

-
- [1] K. Landsteiner, *Acta Phys. Pol. B* **47**, 2617 (2016), 1610.04413.
 - [2] D. E. Kharzeev, K. Landsteiner, A. Schmitt, and H. Yee, *Lect. Notes Phys.* **871**, 1 (2012), 1211.6245.
 - [3] S. L. Adler, *Phys. Rev.* **177**, 2426 (1969).
 - [4] K. Fukushima, D. E. Kharzeev, and H. J. Warringa, *Phys. Rev. D* **78**, 074033 (2008), 0808.3382.
 - [5] M. A. Metlitski and A. R. Zhitnitsky, *Phys. Rev. D* **72**, 045011 (2005), hep-ph/0505072.
 - [6] G. M. Newman and D. T. Son, *Phys. Rev. D* **73**, 045006 (2006), hep-ph/0510049.
 - [7] V. Skokov, P. Sorensen, V. Koch, S. Schlichting, J. Thomas, S. Voloshin, G. Wang, and H. Yee, *Chin. Phys. C* **41**, 072001 (2017), 1608.00982.
 - [8] CMS Collaboration, *Phys. Rev. C* **97**, 044912 (2018), 1708.01602.
 - [9] D. Blaschke, J. Aichelin, E. Bratkovskaya, V. Friese, M. Gazdzicki, J. Randrup, O. Rogachevsky, O. Teryaev, and V. Toneev, *Eur. Phys. J. A* **52**, 267 (2016).
 - [10] J. Adam et al. (STAR Collaboration), “Charge separation measurements in p(d)+Au and Au+Au collisions; implications for the chiral magnetic effect,” (2020), 2006.04251.
 - [11] R. A. Lacey and N. Magdy, “Quantification of the Chiral Magnetic Effect in Au+Au collisions at $\sqrt{s_{NN}} = 200$ geV,” (2020), 2006.04132.
 - [12] J. Zhao and F. Wang, *Prog. Part. Nucl. Phys.* **107**, 200 (2019), 1906.11413.
 - [13] L. Huang, M. Nie, and G. Ma, *Phys. Rev. C* **101**, 024916 (2020), 1906.11631.
 - [14] A. Bzdak, V. Koch, and J. Liao, *Lect. Notes Phys.* **871**, 503 (2013), 1207.7327.
 - [15] D. E. Kharzeev and J. Liao, *Nucl. Phys. News* **29**, 26 (2019).
 - [16] STAR Collaboration: J. Adam et al., “Methods for a blind analysis of isobar data collected by the STAR collaboration,” (2019), 1911.00596.
 - [17] D. A. Teaney, *Quark-Gluon Plasma* **4**, 207 (2010), 0905.2433.
 - [18] S. A. Voloshin (STAR Collaboration), *Indian J. Phys.* **85**, 1103 (2011), 0806.0029.
 - [19] F. Becattini, I. Karpenko, M. Lisa, I. Upsal, and S. Voloshin, *Phys. Rev. C* **95**, 054902 (2017), 1610.02506.
 - [20] Y. Jiang, S. Shi, Y. Yin, and J. Liao, *Chin. Phys. C* **42**, 011001 (2018), 1611.04586.
 - [21] S. Shi, H. Zhang, D. Hou, and J. Liao, *Nucl. Phys. A* **982**, 539 (2018), 1807.05604.
 - [22] S. Shi, Y. Jiang, E. Lilleskov, and J. Liao, *Ann. Phys.* **394**, 50 (2018), 1711.02496.
 - [23] J. Erdmenger, M. Haack, M. Kaminski, and A. Yarom, *JHEP* **0901**, 055 (2009), 0809.2488.
 - [24] D. T. Son and P. Surowka, *Phys. Rev. Lett.* **103**, 191601 (2009), 0906.5044.
 - [25] N. Banerjee, J. Bhattacharya, S. Bhattacharyya, S. Dutta, R. Loganayagam, and P. Surowka, *JHEP* **1101**, 094 (2011), 0809.2596.
 - [26] X. Guo, D. E. Kharzeev, X. Huang, W. Deng, and Y. Hirono, *Nucl. Phys. A* **967**, 1 (2017), 1704.05375.
 - [27] G. Inghirami, M. Mace, Y. Hirono, L. Del Zanna, D. E. Kharzeev, and M. Bleicher, *Eur. Phys. J. C* **80**, 293 (2020), 1908.07605.
 - [28] G. Liang, J. Liao, S. Lin, L. Yan, and M. Li, “Chiral magnetic effect in isobar collisions from stochastic hydrodynamics,” (2020), 2004.04440.
 - [29] A. V. Sadofyev and M. V. Isachenkov, *Phys. Lett. B* **697**, 404 (2011), 1010.1550.
 - [30] E. V. Gorbar, V. A. Miransky, I. A. Shovkovy, and X. Wang, *Phys. Rev. D* **88**, 025025 (2013), 1304.4606.
 - [31] S. Golkar and D. T. Son, *JHEP* **02**, 169 (2012), 1207.5806.
 - [32] K. Jensen, P. Kovtun, and A. Ritz, *JHEP* **1310**, 186 (2013), 1307.3234.
 - [33] U. Gursoy and A. Jansen, *JHEP* **1410**, 92 (2014), 1407.3282.
 - [34] A. Jimenez-Alba and L. Melgar, *JHEP* **10**, 120 (2014), 1404.2434.
 - [35] A. Avdoshkin, A. V. Sadofyev, and V. I. Zakharov, *Phys. Rev. D* **97**, 085020 (2018), 1712.01256.
 - [36] A. Yamamoto, *Phys. Rev. Lett.* **107**, 031601 (2011), 1105.0385.
 - [37] V. Braguta, M. N. Chernodub, V. A. Goy, K. Landsteiner, A. V. Molochkov, and M. I. Polikarpov, *Phys. Rev. D* **89**, 074510 (2014), 1401.8095.
 - [38] M. Pühr and P. V. Buividovich, *Phys. Rev. Lett.* **118**, 192003 (2017), 1611.07263.
 - [39] Y. Burnier, D. E. Kharzeev, J. Liao, and H. Yee, *Phys. Rev. Lett.* **107**, 052303 (2011), 1103.1307.
 - [40] D. E. Kharzeev and H. Yee, *Phys. Rev. D* **83**, 085007 (2011), 1012.6026.
 - [41] C. Gattringer and K. Langfeld, *Int. J. Mod. Phys. A* **31**, 1643007 (2016), 1603.09517.
 - [42] J. B. Kogut, D. K. Sinclair, S. J. Hands, and S. E. Morrison, *Phys. Rev. D* **64**, 094505 (2001), hep-lat/0105026.
 - [43] J. B. Kogut, M. A. Stephanov, D. Toublan, J. J. M. Verbaarschot, and A. Zhitnitsky, *Nucl. Phys. B* **582**, 477 (2000), hep-ph/0001171.
 - [44] P. V. Buividovich, L. von Smekal, and D. Smith, *Phys. Rev. D* **102**, 094510 (2020), 2007.05639.
 - [45] T. Boz, P. Giudice, S. Hands, and J. Skullerud, *Phys. Rev. D* **101**, 074506 (2020), 1912.10975.
 - [46] J. Wilhelm, L. Holicki, D. Smith, B. Wellegehausen,

- and L. von Smekal, *Phys. Rev. D* **100**, 114507 (2019), 1910.04495.
- [47] L. Holicki, J. Wilhelm, D. Smith, B. Wellegehausen, and L. von Smekal, *PoS LATTICE2016*, 052 (2017), 1701.04664.
- [48] T. Boz, P. Giudice, S. Hands, J. Skullerud, and A. G. Williams, *AIP Conf. Proc.* **1701**, 060019 (2016), 1502.01219.
- [49] S. Cotter, P. Giudice, S. Hands, and J. Skullerud, *Phys. Rev. D* **87**, 034507 (2013), 1210.4496.
- [50] N. Strodthoff, B. Schaefer, and L. von Smekal, *Phys. Rev. D* **85**, 074007 (2012), 1112.5401.
- [51] N. Strodthoff and L. von Smekal, *Phys. Lett. B* **731**, 350 (2014), 1306.2897.
- [52] L. McLerran and R. D. Pisarski, *Nucl. Phys. A* **796**, 83 (2007), 0706.2191.
- [53] V. V. Braguta, E. Ilgenfritz, A. Y. Kotov, A. V. Molochkov, and A. A. Nikolaev, *Phys. Rev. D* **94**, 114510 (2016), 1605.04090.
- [54] I. Amado, K. Landsteiner, and F. Pena-Benitez, *JHEP* **05**, 081 (2011), 1102.4577.
- [55] R. Kaiser and H. Leutwyler, *Eur. Phys. J. C* **17**, 623 (2000), hep-ph/0007101.
- [56] E. Berkowitz, D. Brantley, C. Bouchard, C. Chang, M. A. Clark, N. Garron, B. Joo, T. Kurth, C. Monahan,

- H. Monge-Camacho, A. Nicholson, K. Orginos, E. Rinaldi, P. Vranas, and A. Walker-Loud, “An accurate calculation of the nucleon axial charge with lattice QCD,” (2017), 1704.01114.
- [57] R. G. Edwards, G. T. Fleming, P. Hagler, J. W. Negele, K. Orginos, A. Pochinsky, D. B. Renner, D. G. Richards, and W. Schroers, *Phys. Rev. Lett.* **96**, 052001 (2006), hep-lat/0510062.
- [58] A. Hasenfratz and F. Knechtli, *Phys. Rev. D* **64**, 034504 (2001), hep-lat/0103029.
- [59] M. Bochicchio, L. Maiani, G. Martinelli, G. C. Rossi, and M. Testa, *Nucl. Phys. B* **262**, 331 (1985).
- [60] V. Furman and Y. Shamir, *Nucl. Phys. B* **439**, 54 (1995), hep-lat/9405004.
- [61] P. V. Buividovich, *Nucl. Phys. A* **925**, 218 (2014), 1312.1843.

Appendix A: Momentum-dependent Chiral Separation Effect for free quarks in the continuum at finite temperature

For free Dirac fermions, the axial-vector current-current correlator in (2) is given by the one-loop integral of the form [61]:

$$\langle j_\mu^A(k) j_\nu^V(-k) \rangle = T \sum_{l_0} \int \frac{d^3 l}{(2\pi)^4} \frac{\text{Tr}(\gamma_\mu \gamma_5 (m - i\gamma_\alpha (l_\alpha + k_\alpha/2)) \gamma_\nu (m - i\gamma_\beta (l_\beta - k_\beta/2)))}{((l + k/2)^2 + m^2)((l - k/2)^2 + m^2)}, \quad (\text{A1})$$

where \sum_{l_0} denotes summation over fermionic Matsubara frequencies $l_0 = 2\pi T(n + 1/2) - i\mu$ (shifted into the complex plane in order to account for the chemical potential μ). We explicitly substitute the values $\mu = 1$, $\nu = 2$, $k = (0, 0, 0, k_3)$ and represent the integrand as a sum of simple fractions of the form $\frac{1}{l_0 - i\mu_V \pm i\sqrt{(\vec{l} \pm \vec{k}/2)^2 + m^2}}$ (see

e.g. Appendix A in [61] for the full derivation). The time-like momentum l_0 can then be summed over using the identity

$$T \sum_{l_0} \frac{1}{l_0 - i\epsilon} = \frac{i}{2} \tanh\left(\frac{\epsilon + \mu}{2T}\right). \quad (\text{A2})$$

After some algebraic manipulations, we obtain the following expression which is suitable for numerical integration:

$$\begin{aligned} \langle j_1^A(k_3) j_2^V(-k_3) \rangle &= \frac{i}{2} \int_{-\infty}^{+\infty} \frac{dl_3}{2\pi l_3} \int_0^{+\infty} \frac{dl_\perp^2}{4\pi} \\ &\left(\tanh\left(\frac{\mu + \sqrt{m^2 + l_\perp^2 + (k_3/2 + l_3)^2}}{2T}\right) - \tanh\left(\frac{\mu + \sqrt{m^2 + l_\perp^2 + (k_3/2 - l_3)^2}}{2T}\right) + \right. \\ &\left. + \tanh\left(\frac{\mu - \sqrt{m^2 + l_\perp^2 + (k_3/2 + l_3)^2}}{2T}\right) - \tanh\left(\frac{\mu - \sqrt{m^2 + l_\perp^2 + (k_3/2 - l_3)^2}}{2T}\right) \right), \end{aligned} \quad (\text{A3})$$